Published in final edited form as:
J Immunol. 2008 June 15; 180(12): 8250–8261.

A *Leishmania* Ortholog of Macrophage Migration Inhibitory Factor Modulates Host Macrophage Responses[1]

Daniela Kamir[2,*,¶], **Swen Zierow**[2,*,¶], **Lin Leng**[*], **Yoonsang Cho**[*], **Yira Diaz**[†], **Jason Griffith**[*], **Courtney McDonald**[*], **Melanie Merk**[*,¶], **Robert A. Mitchell**[‡], **John Trent**[‡], **Yibang Chen**[§], **Yuen-Kwan Amy Kwong**[§], **Huabao Xiong**[§], **Jon Vermeire**[*], **Michael Cappello**[*], **Diane McMahon-Pratt**[*], **John Walker**[†], **Jurgen Bernhagen**[¶], **Elias Lolis**[*], and **Richard Bucala**[3,*]

[*]*Yale University School of Medicine, New Haven, CT 06520*

[†]*Centro Internacional de Entrenamiento e Investigaciones Médicas, Cali, Colombia*

[‡]*University of Louisville, Louisville, KY 40202*

[§]*Mt. Sinai School of Medicine, New York, NY 10029*

[¶]*Institute of Biochemistry, University Hospital Rheinisch-Westfaelische Technische Hochschule, Aachen, Germany*

Abstract

Parasitic organisms have evolved specialized strategies to evade immune defense mechanisms. We describe herein an ortholog of the cytokine, macrophage migration inhibitory factor (MIF), which is produced by the obligate intracellular parasite, *Leishmania major*. The *Leishmania* MIF protein, Lm1740MIF, shows significant structural homology with human MIF as revealed by a high-resolution x-ray crystal structure (1.03 Å). Differences between the two proteins in the N-terminal tautomerization site are evident, and we provide evidence for the selective, species-specific inhibition of MIF by small-molecule antagonists that target this site. Lm1740MIF shows significant binding interaction with the MIF receptor, CD74 ($K_d = 2.9 \times 10^{-8}$ M). Like its mammalian counterpart, Lm1740MIF induces ERK1/2 MAP kinase activation in a CD74-dependent manner and inhibits the activation-induced apoptosis of macrophages. The ability of Lm1740MIF to inhibit apoptosis may facilitate the persistence of *Leishmania* within the macrophage and contribute to its evasion from immune destruction.

Leishmaniasis is caused by an obligate, intracellular infection of macrophages with species of the eukaryotic genus *Leishmania*. Promastigotes invade target cells, transform into

[1]This work was supported by National Institutes of Health Grants AI051306 and AI042310 (to R.B.), U19 AI65866−01 (to D.Mc.-P. and R.B.), and AI065029 (to E.L.); Deutsche Forschungsgemeinschaft Grant SFB542/A7 (to J.B.); and fellowships from the Marianne und Dr. Fritz Walter Fischer-foundation im Stifterverband der Deutschen Wissenschaft (to D.K.), the German Academic Exchange Service (to S.Z.), and the Studienstiftung des deutschen Volkes (to M.M.).

3 Address correspondence and reprint requests to Dr. Richard Bucala, Yale University School of Medicine, TAC S525, P.O. Box 208031, 300 Cedar Street, New Haven, CT 06520. E-mail address: E-mail: Richard.Bucala@Yale.edu or Dr. Elias Lolis, Yale University School of Medicine, SHM B345, P.O. Box 208066, 333 Cedar Street New Haven, CT 06520−8066. E-mail address: E-mail: Elias.Lolis@Yale.edu.

[2]D.K. and S.Z. contributed equally to this work.

[4]Abbreviations used in this paper: MIF, macrophage migration inhibitory factor; BMM, bone marrow-derived macrophage; ISO-1, (*S*,*R*)-3-(4-hydroxyphenyl)-4,5-di-hydro-5-isoxazole acetic acid methyl ester; 4-IPP, 4-iodo-phenyl-pyrimidine; Lm1740MIF, *Leishmania major* MIF ortholog 1740; Lm1750MIF, *L. major* MIF ortholog 1750; qPCR, quantitative PCR; sCD74, soluble CD74; SNP, sodium nitroprusside; FWD, forward; BWD, backward.

Disclosures
The authors have no financial conflict of interest.

amastigotes, and become established within the phagolysosome (1). Although resident in macrophages, the parasite avoids triggering antimicrobial responses; however, it may be eliminated over time with the development of an effective adaptive immune response (2).

Like all parasites, *Leishmania* protozoa have evolved specialized strategies to evade immune destruction and to complete their life cycle (3). Several host and parasite-specific factors play a role in the persistence of *Leishmania* within infected cells and in influencing the clinical manifestations of the disease, which include nonhealing cutaneous ulcers and visceral involvement. Among these factors, the host cytokine response plays a key role by effecting innate, antimicrobial responses and by promoting the differentiation of a protective T cell response (4).

The recent elucidation of the *Leishmania major* genome (5) has revealed two genes that exhibit significant sequence identity with the mammalian cytokine, macrophage migration inhibitory factor (MIF).[4] MIF is an upstream activator of innate immunity that induces sustained ERK1/2 MAPK activation and protects monocytes/macrophages from activation-induced apoptosis (6). Several primitive eukaryotes encode MIF-like genes that show remarkable similarity to the mammalian counterpart, such as the human parasitic nematodes *Brugia malayi* (7) and *Ancylostoma ceylonicum* (8). The tick vector responsible for the transmission of anaplasmosis, *Amblyomma americanum*, produces an MIF ortholog that is expressed in the salivary gland (9). MIF-like proteins also have been reported recently in pathogenic species of *Eimeria* (10), *Trichinella* (11), and *Plasmodium* (12,13), and the question has been raised as to whether these proteins play a role in the parasite-host interaction.

In this report, we describe the cloning of *L. major* orthologs of MIF and the functional characterization of the ortholog, Lm1740MIF, which shows 22% sequence identity with human MIF. Lm1740MIF was produced recombinantly and crystallographically analyzed at a resolution of 1.03 Å. Lm1740MIF interacts functionally with the MIF receptor, CD74, and exhibits an antiapoptotic activity that may facilitate the intracellular persistence of *Leishmania* in macrophages.

Materials and Methods

Mice

Mice (BALB/c, C3H/HeJ, and C3H/HeN) were purchased from Charles River Laboratories. BALB/c mice deficient in the MIF receptor (CD74-KO) were provided originally by Dr. Idit Shachar (Weizmann Institute, Rehovot, Israel; Ref. 14). All mice were used at 6−8 wk of age, and experiments were performed in accordance with the Yale Institutional Animal Care and Use Committee guidelines.

Parasite and cell cultures

Bone marrow macrophages (BMM) were harvested from mouse femurs and cultured for 4 days with complete medium containing RPMI 1640 (Life Technologies), 20% FBS (Life Technologies), 30% L929-conditioned medium, and 1% penicillin/streptomycin (Life Technologies). On day 5, cells were replated at a density of 4×10^6/ml and treated according to the intended experiments. Peritoneal exudate cells were obtained from mice that were injected 3−4 days previously with 2 ml of 4% sterile thioglycolate broth (15). *L. major* (MHOM/IL/79/LRC-L251; Ref. 16) promastigotes were cultured at 23°C in complete Schneider's medium supplemented with 20% heat-inactivated FBS and gentamicin (10 μg/ml; Invitrogen).

Sequence and phylogenetic analyses

Phylogenetic analyses were conducted using sequences from the ClustalW multiple alignment output and the Neighbor-Joining method (17) via the MEGA3.1 interface (18) with the following settings for DNA phylogenetic analysis. Pairwise alignment parameters: gap opening penalty, 15; gap extension penalty, 6.66; multiple alignment: gap opening penalty, 15; gap extension penalty, 6.66; delay divergent cutoff, 30%; DNA transition weight, 30%; weight matrix IUB with 5000 bootstrap replicates. For protein phylogenetic analysis, the following settings were chosen. Pairwise alignment parameters: gap opening penalty, 10; gap extension penalty, 0.1; multiple alignment: gap opening penalty, 10; gap extension penalty, 0.2; Gonnet protein weight matrix and delay divergent cutoff, 30%. To compare identity, the Expert Protein Analysis System (ExPASy) proteomics server of the Swiss Institute of Bioinformatics was used. The interface T-Coffee (19) was used for sequence alignment, and the residues are numbered in accordance with the alignment; gaps are counted.

PCR analyses

Total RNA from *L. major* was isolated from procyclic, metacyclic cultures and from homogenized infected mice lymph nodes (amastigotes) using Trizol (Invitrogen) and reverse-transcribed using the AccuScript Kit from Stratagene. To isolate metacyclics, a purification over a Percoll gradient (Invitrogen) was conducted. The RT-PCR amplifications consisted of a denaturation step (94°C, 1 min), an annealing step (50°C, 2 min), and an elongation step (72° C, 3 min). For the last cycle, the elongation step was extended to 10 min at 72°C. Reactions were conducted for 32 cycles. *L. major* ADP/ATP carrier (LmjF19.0210; Ref. 20) and rRNA45 (CC144545; Ref. 21) transcripts served as internal controls. The amplification primers were: Lm1740 forward (FWD), 5′-ATGCCGGTCATTCAAACG-3′; Lm1740 backward (BWD) 2, 5′-CTCTGGTTTGCCGAGTACA-3′; Lm1750FWD, 5′-ATGCCGTTTCTGCAGAC-3′; Lm1750BWD2, 5′-AGTCATCACGAAGTCCTC-3′; carrier FWD, 5′-ATCTCATACCCGC TGGACAC-3′; carrier BWD, 5′-TCAAGCGAGTTGCGGTAGTT-3′; rRNA45FWD, 5′-CCTACCATGCCGTGTCCTTCTA-3′; and rRNA45BWD, 5′-AACGACCCCTGCAGCAATAC-3′.

Real-time quantitative PCR (qPCR) was performed with a DNA SYBR Green kit according to the manufacturer's instructions (Roche). Amplification for Lm1740MIF and Lm1750MIF was conducted for 3 min at 95°C and 30 s at 95°C followed by 30 s at 60°C for 40 cycles. Amplification for ADP/ATP carrier and rRNA45 was conducted for 3 min at 95°C and 30 s at 95°C followed by 30 s at 62°C for 40 cycles. The linearity of the assays was ensured by performing serial dilutions of the templates for each primer set. The mean normalized expression values were calculated from the obtained threshold cycle and their respective standard curve slopes with the qgene software (22).

Molecular cloning of L. major *MIF*

Two forward primers, Lm1740FWD and Lm1750FWD, and two backward primers, Lm1740BWD, 5′-TTA GAA GTT TGT GCC ATT CC-3′ and Lm1750BWD, 5′-TCA AAA GTT AGT GCC GTT-3′ were synthesized. The nucleotide lengths of the amplified DNA products were each 342 bp. Each PCR product was cloned into the 3′-TdR site of the linearized vector pCR2.1 (Invitrogen), transformed into the *Escherichia coli* TOP10F′-competent cells (Invitrogen), and selected by blue-white screening. The predicted sequences of the clones were confirmed by bidirectional DNA sequencing. The recombinant plasmids were isolated using Minipreps (Promega) and purified from 2% agarose gels. The Lm1740MIF and Lm1750MIF DNA sequences then were subcloned into pcDNA3.1/V5-His TOPO (Invitrogen) for eukaryotic expression studies, and Lm1740MIF was additionally subcloned into the prokaryotic expression vector pCRT7/CT-TOPO (Invitrogen) for recombinant protein

production. A stop codon was engineered immediately 3′ to the coding region to exclude the expression of the V5-His C-terminal tag.

Expression and purification of Lm1740MIF

Recombinant, native sequence Lm1740MIF protein was expressed in BL21(DE3) *E. coli* and induced with isopropyl-D-thiogalactoside. After 4 h, the cells were harvested, washed twice in 30 mM Bis-Tris (pH 6.8), 20 mM NaCl, and resuspended at 2.5% of the original volume of growth medium. Cells were lysed in the presence of protease inhibitor mixture (Roche) using a French press. To ensure a low endotoxin (LPS) content, all buffers used for purification of Lm1740MIF were prepared using endotoxin-free HyPure Cell Culture Grade Water (<0.005 endotoxin U/ml; Hy-Clone). Columns were treated in three cycles with 2 column volumes of 1 M NaOH followed by 2 column volumes of pyrogen-free water. Soluble Lm1740MIF protein was purified sequentially by anion exchange chromatography using Q-Sepharose Fast Flow resin (Amersham Bioscience) with a linear salt gradient from 30 mM Bis-Tris (pH 6.8), 20 mM NaCl to 30 mM Bis-Tris (pH 6.8), 400 mM NaCl, followed by a linear pH gradient from 30 mM Bis-Tris (pH 6.8), 20 mM NaCl to 20 mM citric buffer (pH 5.5), 20 mM NaCl. The residual impurities were removed by gel filtration over an S-75 column (HiLoad 16/60 Superdex 75; Amersham Bioscience) and eluted with 30 mM Bis-Tris (pH 6.8), 20 mM NaCl. The final purity of the MIF product was >98.0% as estimated by SDS-PAGE stained with Coomassie. The resulting Lm1740MIF preparations contained <20 pg of LPS per μg of protein as quantified by the PyroGene Recombinant Factor C assay (Cambrex BioScience). Recombinant human and murine MIF was prepared as described by Bernhagen et al. (23).

Crystallization and structure determination

Native and selenomethionylated Lm1740MIF were expressed and purified as described and concentrated to 8 mg/ml. Crystals were obtained by the hanging drop vapor diffusion method at 18°C. The reservoir solution for the native protein included 0.1 M HEPES-Na (pH 7.5), 20% (v/v) isopropanol, and 20% (w/v) polyethylene glycol 4000. The reservoir solution for the selenomethionylated protein included 0.1 M trisodium citrate dihydrate (pH 5.6), 10% (v/v) isopropanol, and 20% (w/v) polyethylene glycol 4000. Crystallization drops were prepared by combining equal volumes of protein solution and reservoir solution. Native crystals appeared within 3 wk, whereas the seleneomethionylated crystals grew overnight. For data collection, the crystals were cryoprotected in the reservoir solution with 20% glycerol. Diffraction data were collected at beamline X29A in the Brookhaven National Laboratory. Multiple wavelength anomalous diffraction data of a selenomethionylated crystal were collected at three different wavelengths (0.97912 Å, 0.97928 Å, and 0.96389 Å), and a native crystal was used to collect data at a single wavelength (0.95 Å) to a resolution of 1.03 Å. The data were indexed in space group R3 ($a = b = 52.3$ Å, $c = 96.8$ Å) and scaled using HKL2000 (24).

The initial phase was determined with the MAD data using HKL2MAP (25). The human MIF structure (26) was used as a template to build a Lm1740MIF model using XTALVIEW (27). The model was refined against the native data using REFMAC (28) and CNS (29) followed by SHELX-97 (30). XTALVIEW was used to visualize the structure and to make manual adjustments of the coordinates to improve their agreement with the electron density map. Crystallographic data collection and refinement statistics are listed in Table I. The coordinates of the Lm1740MIF structure have been deposited with the Protein Data Bank under accession code 3B64.

Cellular uptake studies

Fluorescein labeling was performed with *N*-hydroxysuccinimide ester-fluorescein as described by manufacturer (Pierce). For uptake studies, murine RAW264.7 macrophages cultured on glass cover slides were incubated with MIF or Lm1740MIF (1.5 μM) for 30 min at 37°C. Cells

were washed three times with PBS and three times with 50 mM glycine, PBS, and then fixed for 20 min at 37°C with 3.7% formaldehyde, 0.1% Triton X, PBS solution. Actin was visualized with Texas Red-X phalloidin (Invitrogen).

Mass spectrometry

Recombinant Lm1740MIF protein was analyzed by electrospray using a C-4 capillary column and a Q-Tof Micro mass spectrometer at the Proteomics and Mass Spectrometry Resource of the Yale Keck Laboratory (New Haven, CT). Solvent A was 5% acetonitrile, 0.1% formic acid, and 0.02% trifluoroacetic acid. Solvent B consisted of 95% acetonitrile, 0.1% formic acid, and 0.02% trifluoroacetic acid. The flow rate was 5 μl/min. The mass measurement accuracy of this instrumentation was ± 0.01−0.02%.

D-Dopachrome tautomerization assay

The model MIF substrate, D-dopachrome methyl ester (2.4 mM), was prepared as described previously (31). Tautomerase activity was determined at room temperature by adding a final concentration of 0.75 mM D-dopachrome methyl ester (ε = 3700 M^{-1} cm^{-1}) (32) to a 96-well plate containing human MIF or Lm1740MIF in 40 mM potassium phosphate buffer (pH 7.4). The inhibitory effect of (*S*,*R*)-3-(4-hydroxyphenyl)-4,5-dihydro-5-isoxazole acetic acid methyl ester (ISO-1) or 4-iodophenylpyrimidine (4-IPP) was determined by preincubating LmMIF1740 or human MIF with inhibitor for 30 min before addition of the substrate. The initial velocity of the MIF-mediated conversion of D-dopachrome methyl ester to indolecarboxylic acid methyl ester was measured for 30 s at λ = 475 nm, and the specific activity was expressed as converted dopachrome in millimols per minute per micromolar concentration of protein.

Migration studies

Migration assays were performed as previously described (8). Briefly, human PBMCs were isolated from whole blood, washed, and resuspended in RPMI 1640 to 1×10^6 cells/ml. Aliquots then were placed in the upper chamber of a 24-well cell culture insert with 8-μm pore size (Falcon). In the lower chamber, MIF or Lm1740MIF was placed after a 30-min preincubation with test compounds. The MIF inhibitors included ISO-1 and 4-IPP. After incubation for 3 h at 37°C, 5% CO_2-transmigrated cells were methanol fixed, stained with Giemsa, and counted under light microscopy.

MIF receptor binding studies

The binding of Lm1740MIF to the MIF cell surface receptor was studied by coating individual wells of a 96-well plate with recombinant, soluble CD74 ectodomain ($sCD74^{73-232}$) as described by Leng et al. (33). Plates were washed 4 times with TTBS (pH 7.4) and blocked with superblock buffer (Pierce) for two hrs at room temperature. Human MIF was biotinylated (Roche) and added at 2 μg/ml in triplicate wells with decreasing concentrations of human MIF, heat-denatured human MIF, Lm1740MIF, or a blocking Ab directed against the MIF receptor ectodomain (clone LN2) (33). Incubation was continued at room temperature for 2 h followed by washing with TTBS (pH 7.4). The bound, biotinylated hMIF was detected by adding streptavidin-conjugated alkaline phosphatase for 1 h, followed by washing and detection with *p*-nitrophenyl phosphate (Sigma-Aldrich). OD_{405} was measured using a kinetic microplate reader and values plotted as percent OD_{405} relative to wells containing biotinylated human MIF alone. Each plot represents at least three independently performed assays, and each data point depicts a SEM ≤ 10%.

The real-time binding interaction of Lm1740MIF with CD74 was measured by surface plasmon resonance using a BIAcore 2000 optical biosensor (BIAcore) as previously described (33). The

CM5 sensor chips and the BIA Evaluation software were from GE Healthcare. The MIF receptor ectodomain ($sCD74^{73-232}$) was immobilized according to manufacturer's instructions using the Biacore Amine Coupling Kit. Briefly, $sCD74^{73-232}$ was diluted in 10 mM sodium acetate (pH 5.2) at 1 μmol. Fifty microliters of a *N*-hyrdoxysuccinimide and *N*-ethyl-*N*-(dimethyaminopropyl)carbodiimide mixture was injected at a speed of 2 μl/min for 25 min, followed by injection of 50 μl of 1 μM purified $sCD74^{73-232}$. Once the surface plasmon resonance reached 10,000 U, the injection was stopped, and the active amine sites were blocked with 35 μl of 1 M ethanolamine (pH 8.5). The immobilized CM5 chip was washed overnight with 1× PBS at 20 μl/min. The derived sensor chips were washed and equilibrated in HEPES or PBS (pH 8.0; 20 μl/min), and the ligand (Lm1740MIF) was introduced at five serial dilutions in BIAcore buffer (1 mM DTT, 2.5 mM $MgCl_2$, 20 mM HEPES, 1 mM EDTA, 150 mM NaCl, 0.005% P20) in 60- to 100-μl injection volumes at a flow rate of 20 μl/min. Binding was measured at 25°C for 5 min, followed by 15 min of dissociation. Sensor chip regeneration was performed for 1 min with 1 M NaCl, 50 mM NaOH. The whole process was repeated three times for each dilution sample. Sensorgram response data were analyzed in the BIA evaluation kinetics package and the equilibrium binding constants calculated.

Apoptosis studies

Transfection of Lm1740MIF and Lm1750MIF eukaryotic expression plasmids into the murine RAW264.7 monocyte cell line was performed using a Nucleofector (Amaxa) and the T-20 program described by the manufacturer. Briefly, 2.5×10^6 cells were resuspended in 100 μl of Nucleofector solution together with 2 μg of plasmid DNA. After the pulse, 500 μl of DMEM, 10% FBS was added, and the cells were seeded into 24-well plates for apoptosis studies. Apoptosis was induced with the NO donor, sodium nitroprusside (SNP). Transfection efficiencies were typically 30% ($n > 3$ studies) and were measured by fluorescence microscopy at 24 h posttransfection with 2 μg of pmaxGFP (Amaxa). BMMs (4×10^6) were cultured in 20-mm plates, treated with murine MIF or Lm1740MIF, and incubated overnight with and without SNP (Amersham Biosciences) (35). Apoptosis was quantified by ELISA for cytoplasmic histone-associated DNA fragments (Roche). Cytoplasmic p53 content was analyzed by immunoblotting with a pair of phospho-p53 (Ser^{15}) and total p53 Abs (Cell Signaling Technology) according to the manufacturer's instructions. The secondary Ab was an anti-rabbit IgG Ab conjugated to HRP (Cell Signaling Technology), and detection was by chemiluminescence (GE Healthcare). The blots displayed are representative of stimulation studies that were performed at least three times.

Signal transduction studies

Mouse BMMs and mouse thioglycolate-elicited peritoneal macrophages (4×10^6/plate) were rendered quiescent by incubation in 0.1% FBS before stimulation with MIF for 2 h (36). Apoptosis was induced with SNP. Negative controls were conducted by not stimulating cell death with SNP. Cells were lysed in buffer containing 20 mM HEPES (pH 7.4), 50 mM β-glycerolphosphate, 2 mM EGTA, 1 mM DTT, 10 mM NaF, 1 mM $NaVO_4$, 10% glycerol, 1% Triton X-100, and freshly added protease inhibitors (Complete, Mini, EDTA-free; Roche). For immunoblotting, cell lysates were separated by 10% SDS-PAGE and transferred to PVDF Immobilon-P transfer membranes (Millipore). Immunoblotting was conducted with Abs directed against total ERK1/2 (Santa Cruz Biotechnology), and phospho-ERK-1/2 (Cell Signaling Technology) according to the manufacturer's instructions. The secondary Ab was an anti-rabbit IgG Ab conjugated to HRP (Cell Signaling Technology), and detection was by chemiluminescence (GE Healthcare). The blots displayed are representative of stimulation studies that were performed at least three times.

Results

Sequence alignment and phylogenetic analyses

Two genetic loci, *Lm1740* and *Lm1750*, were identified in the recently completed *L. major* genome (5) to have a potential open reading frame (342 bp) with 22% identity with human MIF. By computational comparison with other *Leishmania* and *Trypanosoma* genes (37), both a consensus TATA-box and a polyadenylation signal sequence were evident in the flanking regions of these loci (Fig. 1*A*). The two putative *L. major MIF* orthologs (Lm1740MIF and Lm1750MIF) were predicted to encode a 112-aa protein after excision of the initiating methionine residue. Similar to other MIF orthologs that have been described (7-9,12,13), the *Leishmania* MIF-like genes do not contain an N-terminal, secretory signal sequence.

Phylogenetic analysis using the Neighbor-Joining method for both DNA and protein sequences produced similar results, of which the latter is displayed in Fig. 1*B*. Gene duplication would be a likely origin for MIF paralogs within the same organism, as in the case of the two *L. major* and *Leishmania infantum* MIF-related sequences. Lm1740MIF showed 58−99% sequence identity with MIF-like genes in other *Leishmania* species and 22−31% sequence identity with mammalian MIFs. Except for some branch rearrangements, few differences were observed between the topology of the MIF DNA and protein phylograms (data not shown).

An amino acid sequence alignment of 12 selected members of the MIF protein family was prepared using the T-Coffee multiple sequence alignment program (Fig. 1*C*). Altogether, there are nine invariant residues in MIF (Pro^{1}, Leu^{21}, Gly^{34}, Lys^{35}, Pro^{36}, Phe^{52}, Gly^{54}, Gly^{68}, and Phe^{116}). Mammalian MIF is distinguished by the presence of three conserved cysteines (Cys^{59}, Cys^{62}, and Cys^{83}), the first two of which define a CXXC motif that mediates thiol-protein oxidoreductase activity (38). These conserved cysteines, as well as the CXXC motif, are absent in the *L. major* sequences. The MIF N-terminal proline (Pro^{1}) by contrast appears strictly conserved, with the exception of the grossly truncated *Leishmania braziliensis* sequence. Proline-1 functions as a catalytic base in the tautomerization of model substrates (whether a physiological substrate exists is unknown; see Ref. 38), and this residue has been shown by x-ray crystallography studies of the mammalian proteins to reside within a hydrophobic, substrate-binding pocket (31,39,40).

Expression and cloning of L. major *MIF*

We confirmed the expression of the Lm1740MIF and Lm1750MIF genes in vivo by RT-PCR analysis (data not shown) of total RNA prepared from *L. major* promastigotes (strain MHOM/IL/79/LRC-L251; Ref. 16). By qPCR, procyclic forms were observed to express more MIF than the metacyclic or amastigote forms, the latter of which were detected within the lymph nodes of infected mice (Fig. 2). The difference in the expression levels of Lm1740MIF and Lm1750MIF was quantified with respect to two housekeeping genes, *rRNA45* and *ADP-ATP carrier*.

The Lm1740MIF and Lm1750MIF DNA sequences were subcloned into the eukaryotic expression vector, pcDNA3.1/V5-His TOPO. Lm1740MIF DNA was additionally subcloned into the prokaryotic-expression vector pCRT7/CT-TOPO for recombinant protein production. The coding region was engineered with a 3′ stop codon to exclude the expression of the 3′-epitope tags present in the plasmid vectors and to ensure the production of native sequence protein. We considered native sequence to be important for activity studies because covalent modification of the N-terminal proline inhibits the tautomerase activity of the protein and the C terminus mediates subunit oligomerization (26,31). Recombinant Lm1740MIF protein was purified by sequential fast protein liquid chromatography following procedures adapted from the method of Bernhagen et al. (23) and yielded 15 mg of protein per liter of *E. coli* culture.

Final purification to homogeneity was achieved by gel filtration chromatography (Fig. 3*A*). Electrospray ionization of purified Lm1740MIF protein gave an *m/z* of 12383.56, which is within 0.02% of the predicted mass of the translated amino acid sequence (calculated molecular mass, 12381.22 Da; Fig. 3*B*).

Lm1740MIF activity studies

Mammalian MIF tautomerizes model substrates such as D-dopachrome or *p*-hydoxyphenylpyruvate, although the physiological relevance of the tautomerase activity of the protein continues to be debated (38). Site-directed mutagenesis and crystallography studies of human MIF nevertheless have provided significant insight into the structural determinants of this reaction (31,40-42). Pure, recombinant Lm1740MIF tautomerizes D-dopachrome methyl ester, but the specific activity for the reaction is 13-fold lower than that measured for human MIF (Lm1740MIF, 0.25 mM/min/μM; human MIF, 3.35 mM/min/μM; Fig. 3*C*). A low level of tautomerase activity for Lm1740MIF also was observed with the substrate, *p*-hydoxyphenylpyruvate (data not shown).

We next investigated whether Lm1740MIF is sensitive to human MIF-catalytic site inhibitors using the tautomerase assay. As shown in Fig. 3*C*, the competitive inhibitor ISO-1 (43) inhibits human MIF but not Lm1740MIF, suggesting a selective interaction of this compound with the human MIF tautomerization site. By contrast, 4-IPP, which forms a covalent modification of the MIF N-terminal proline (44) (M. Winner, J. Meier, S. Zierow, B. E. Rendon, G. Crichlow, R. Bucala, L. Leng, N. Smith, E. Lolis, J. O. Trent, and R. Mitchell, submitted for publication) inhibits the tautomerization activity of both MIF proteins with a greater inhibitory effect on Lm1740MIF.

Three-dimensional crystal structure of Lm1740MIF

The x-ray crystal structure of Lm1740MIF was solved at 1.03 Å resolution. The structure consists of 1 protomer per asymmetric unit (Fig. 4*A*, *top*) that forms a trimer with two protomers from adjacent asymmetrical units (*bottom*). The superposition of the Cα backbone atoms of each monomer of human MIF and Lm1740MIF results in a root mean square deviation of 1.8 Å (Fig. 4*B*). The tautomerization site of Lm1740MIF shows a distinct difference in the electrostatic potential relative to the human protein (Fig. 4*C*, *top*), which may be due to the proximity of Glu^{65} from protomer A to the catalytic site. The low tautomerase activity of Lm1740MIF may be explained by this difference in electrostatic potential and by a molecular model of substrate docked in the active site of Lm1740MIF (Fig. 4*C*, *bottom*). Lm1740MIF shares with human and mouse MIF two of the five amino acids (Pro^{1} and Lys^{35}) that have been implicated in substrate contact (40); however, three residues are absent. The replacement of Ile^{67} by a Leu in Lm1740MIF is probably less significant because the contact involves a backbone hydrogen bond, whereas the substitution of Tyr^{98} and Asn^{100} by the hydrophobic residues Phe and Leu, respectively, eliminates two side chain hydrogen bonds to the substrate. Although tautomerase activity is reduced in Lm1740MIF, it is notable that the N-terminal region and hydrophic pocket are conserved in all other MIF or D-dopachrome tautomerases that have been characterized.

Lm1740MIF binds to the MIF receptor, CD74

The possibility that Lm1740MIF produced by *L. major* may influence host immunity prompted us to examine the binding of Lm1740MIF to the human MIF receptor. The cytokine MIF activates cells by engaging its cell surface-binding receptor, CD74, and a high-affinity binding interaction between MIF and the CD74 ectodomain ($CD74^{73-232}$ or sCD74) has been demonstrated (33). We first examined the ability of recombinant Lm1740MIF to compete with human MIF for binding to immobilized sCD74 (Fig. 5*A*). Lm1740MIF inhibited the interaction between human MIF and sCD74, but inhibition was not as complete as achieved with human

MIF as a competitor. We measured the equilibrium dissociation constant for the binding of Lm1740MIF to sCD74 by surface plasmon resonance (BIAcore analysis), which measures real-time binding interactions by changes in the refractive index of a biospecific surface. BIAcore measurements revealed a K_d of 2.9×10^{-8} M for the binding between Lm1740MIF and sCD74 (Fig. 5*B*). This contrasts with a previously determined K_d for the binding of human MIF with sCD74 of 9.0×10^{-9} M (33). These data are consistent with the competition data (Fig. 5*A*) and indicate that Lm1740MIF binds to the human MIF receptor with high affinity, albeit with a 3-fold lower K_d than recombinant human MIF. Lm1740MIF also is internalized into target macrophages (Fig. 5*C*), further supporting a potential interaction with host surface proteins.

Lm1740MIF stimulates monocyte migration

Once produced, MIF inhibits macrophage movement (23,45); however, MIF also exerts a chemoattractant effect on mononuclear cells (46). Like human MIF, Lm1740MIF induces the migration of peripheral blood monocytes across a Transwell membrane (Fig. 6). The small-molecule MIF antagonist, ISO-1, binds to the human MIF tautomerization site (43) and inhibits MIF-induced chemoattraction (8). As expected from the non-inhibitory effect of ISO-1 on Lm1740MIF tautomerase function, ISO-1 failed to block mononuclear cell migration induced by the latter protein, whereas the covalent inhibitor, 4-IPP, inhibited migration induced by MIF or Lm1740MIF.

Lm1740MIF activates ERK1/2 MAPK and inhibits monocyte/macrophage apoptosis

Leishmania-infected macrophages survive longer and are more viable than uninfected macrophages (47). An important biological action of the cytokine MIF is to sustain monocyte/macrophage function by inhibiting activation-induced, p53-dependent apoptosis (34). We hypothesized that Lm1740MIF may contribute to parasitism by prolonging the survival of the infected macrophage.

Transient transfection of an MIF-expressing plasmid into RAW264.7 macrophages inhibits apoptosis by an autocrine/paracrine pathway involving the CD74 membrane receptor (34,48). We tested the comparative ability of plasmids encoding murine MIF, Lm1740MIF, and Lm1750MIF to protect from NO-mediated apoptosis in this model system. As shown in Fig. 7*A*, the two *Leishmania* MIF orthologs inhibited apoptosis in a dose-dependent manner, but at levels that were ~30% lower than that of transfected murine MIF.

We next examined whether recombinant Lm1740MIF similarly inhibits apoptosis in BMMs, both to confirm the biological activity of the protein and to assess its ability to influence the responses of host cells when present in the extracellular milieu. The effect of Lm1740MIF was less than that observed with murine MIF (Fig. 7*B*), which is consistent both with the transfection data (Fig. 7*A*) and with the reduced receptor binding activity (Fig. 5, *A* and *B*). MIF signal transduction through CD74 is known to result in the activation of the ERK1/2 MAPK pathway (35), and Lm1740MIF also induced ERK1/2 phosphorylation in primary murine macrophages (Fig. 7*B*). Because ERK1/2 activation in macrophages may be induced by endotoxin (LPS), which is present in trace quantities in recombinant Lm1740MIF (<20 pg of LPS/μg of protein), we additionally tested Lm1740MIF in macrophages from C3H/HeJ mice, which have a loss of function mutation in the LPS receptor, TLR 4 (49). A dose-dependent increase in ERK1/2 phosphorylation in response to Lm1740MIF was observed in these cells as well, arguing against a role for contaminating endotoxin in Lm1740MIF-induced ERK1/2 phosphorylation.

Downstream of ERK1/2 activation, the antiapoptotic action of MIF is associated with a reduction in the intracytoplasmic content of Ser^{15}-phosphorylated p53, which increases in response to NO treatment (35). Protection from apoptosis by Lm1740MIF also was associated

with a diminution in the cellular content of Ser^{15}-phosphorylated p53 (Fig. 7*B*). Although differences in the relative ability of Lm1740MIF vs murine MIF to effect changes in phosphorylation may be evident, quantitative comparisons are difficult to make given the narrow linearity of signals that is apparent by Western blotting. These results nevertheless indicate that Lm1740MIF is biologically active when added to mammalian cells and, like mammalian MIF, stimulates ERK1/2 phosphorylation and reduces the cellular content of phospho-p53.

Finally, we examined the functional requirement for the MIF receptor in Lm1740MIF action by studying the signaling and apoptotic responses of macrophages obtained from mice deficient in the MIF receptor, CD74. Murine MIF was not active in these cells, which is in agreement with prior reports (33,48), and there was no effect of Lm1740MIF with respect to protection from apoptosis, ERK1/2 phosphorylation, or intracellular phospho-p53 content (Fig. 7*C*). These data, taken together, support the conclusion that Lm1740MIF affects host cell responses, and in particular monocyte/macrophage survival, by engaging the MIF cell surface receptor.

Discussion

We describe herein the characterization of *L. major* encoded orthologs of the cytokine, MIF. The Lm1740MIF and Lm1750MIF genes (58% identity) are expressed in significant levels in cultured promastigotes. The two MIF-like sequences show 22% identity when aligned to human MIF and most likely arose by gene duplication. Recombinant, native sequence Lm1740MIF protein was produced for structural and functional studies. An *E. coli* expression system was used because of its high yield, the absence of known posttranslational modifications of MIF, and prior work showing the utility of fast protein liquid chromatography for preparing pure MIF that is low in endotoxin content (23). We cloned Lm1740MIF in a native sequence and not fusion protein form because of the known sensitivity of the N-terminal region to chemical modifications and evidence that the C terminus of the protein forms contacts necessary for stable trimerization (26,31).

The x-ray crystal structure of Lm1740MIF was solved to 1.03 Å, which is the highest resolution of an MIF protein that has been obtained to date. The overall global topology of Lm1740MIF is similar to that of human and murine MIF (26,51), but the catalytic site shows distinctive features. There is a substantial difference in the electrostatic potential within the catalytic site due to the presence of Glu^{65}, and the N-terminal tautomerase site contains three significant amino acid substitutions. These differences likely explain the low tautomerase activity of Lm1740MIF when compared with human MIF, and they prompted us to investigate whether small-molecular MIF inhibitors also discriminate between Lm1740MIF and human MIF. The MIF inhibitor ISO-1 did not affect tautomerase activity or monocyte migration induced by Lm1740MIF. By contrast, 4-IPP inhibited these activities in both Lm1740MIF and human MIF, with stronger inhibition observed in the case of Lm1740MIF. Small-molecule inhibitors of human MIF that are designed to bind to the tautomerase site of the protein and interfere with biological function are presently in preclinical development (52). Given the structural and functional differences in the tautomerase sites of the human vs the *Leishmania* MIF proteins, it is possible that inhibitors may be designed to interfere selectively with *Leishmania* MIF.

Lm1740MIF bound with high affinity to the MIF receptor ectodomain, as assessed both by an in vitro competition assay and by BIAcore analysis. Although the surface contacts between MIF and the CD74 surface receptor remain unknown, the N-terminal region appears to play an important role in these interactions MIF (44). Nevertheless, there is sufficient structural homology between Lm1740MIF and human MIF to allow for high affinity binding to CD74. The interaction between Lm1740MIF and CD74 led to an equal signal transduction response in macrophages obtained from WT and C3H/HeJ mice, indicating that signaling was not due

to the presence of trace quantities of contaminating endotoxin. Lm1740MIF was active in three functional assays, monocyte migration, ERK1/2 signaling, and protection from apoptosis, although the level of activity was generally lower than for mammalian MIF and appeared consistent with the lower K_d of Lm1740MIF for the CD74 receptor. As in the case of mouse MIF, protection from apoptosis was strictly dependent on CD74, and the response was associated with a decrease in the cytoplasmic content of Ser^{15}-phosphorylated p53.

The present results indicate that a *Leishmania* ortholog of the cytokine MIF has the ability to activate the human MIF receptor and influence the functional responses of monocytes/macrophages. Because *Leishmania* is an intracellular infection of the monocyte/macrophage, it may be hypothesized that one function of *Leishmania*-encoded MIF is to sustain monocyte/macrophage survival and contribute to the persistence of the parasite so that it may complete its infectious life cycle. The precise cellular pathway by which Lm1740MIF activates CD74 remains to be investigated; for instance, the protein may be secreted from infected cells (53) and bind to cell surface CD74, or it may engage CD74 intracellularly by gaining access to the endosomal compartment (54). An additional question posed by these findings is whether there exist further, functional roles for *Leishmania* MIF with respect to the host-parasite interaction. MIF binding to CD74 has been shown recently to lead to the recruitment and activation of additional signaling proteins, including CD44 (48) and the chemokine receptors CXCR2 and CXCR4 (47). Whether Lm1740MIF modulates additional pathways important for intracellular parasitism or for immune evasion remains to be determined. It also is notable that although host-derived MIF may augment the killing of *L. major*, its specific activity is low in comparison to cytokines such as IFN-γ (55).

Although our data are consistent with a role for *Leishmania* MIF in modulating the host immune response, they do not exclude the possibility of an intrinsic function for Lm1740MIF in the growth or replication of the parasite. We note that two *mif*-like genes have been described to be transcriptionally up-regulated in the dauer stage of the free-living nematode, *Caenorhabditis elegans* (56). It has been hypothesized that these genes may have a homeostatic role during adverse conditions that cause developmental arrest (56). A physiological role for *Leishmania* MIF in the parasite life cycle and a closer examination of whether these proteins function as virulence factors may be attained by creating strains of *Leishmania* lacking different MIF orthologs. Such studies also may provide support for the selective, pharmacological targeting of *Leishmania* MIF for therapeutic benefit.

Acknowledgments

We thank Ji Li for helpful scientific discussions and Cedric Notredame and Barry G. Hall for answering unhesitatingly our bioinformatical questions. The technical assistance of K. Goldsmith-Pestana is gratefully acknowledged.

References

1. Chang KP, Dwyer DM. Multiplication of a human parasite (*Leishmania donovani*) in phagolysosomes of hamster macrophages in vitro. Science 1976;193:678–680. [PubMed: 948742]
2. Olivier M, Gregory DJ, Forget G. Subversion mechanisms by which *Leishmania* parasites can escape the host immune response: a signaling point of view. Clin. Microbiol. Rev 2005;18:293–305. [PubMed: 15831826]
3. Bogdan C, Rollinghoff M. The immune response to *Leishmania*: mechanisms of parasite control and evasion. Int. J. Parasitol 1998;28:121–134. [PubMed: 9504340]
4. Schartonkersten T, Scott P. The role of the innate immune-response in Th1 cell-development following *Leishmania major* infection. J. Leukocyte Biol 1995;57:515–522. [PubMed: 7722408]
5. Ivens AC, Peacock CS, Worthey EA, Murphy L, Aggarwal G, Berriman M, Sisk E, Rajandream MA, Adlem E, Aert R, et al. The genome of the kinetoplastid parasite, *Leishmania major*. Science 2005;309:436–442. [PubMed: 16020728]

6. Calandra T, Roger T. Macrophage migration inhibitory factor: a regulator of innate immunity. Nat. Rev. Immunol 2003;3:791–800. [PubMed: 14502271]
7. Pastrana DV, Raghavan N, Fitzgerald P, Eiseinger SW, Metz C, Bucala R, Scleimer RP, Bickel C, Scott AL. Filarial nematode parasites secrete a homologue of the human cytokine macrophage migration inhibitory factor (MIF). Infect Immun 1998;66:5955–5963. [PubMed: 9826378]
8. Cho YS, Jones BF, Vermeire JJ, Leng L, DiFedele L, Harrison LM, Xiong HB, Kwong YKA, Chen Y, Bucala R, et al. Structural and functional characterization of a secreted hookworm macrophage migration inhibitory factor (MIF) that interacts with the human MIF receptor CD74. J. Biol. Chem 2007;282:23447–23456. [PubMed: 17567581]
9. Jaworski DC, Jasinskas A, Metz CN, Bucala R, Barbour AG. Identification and characterization of a homologue of the pro-inflammatory cytokine macrophage migration inhibitory factor in the tick, *Amblyomma americanum*. Insect Mol. Biol 2001;10:323–331. [PubMed: 11520355]
10. Miska KB, Fetterer RH, Lillehoj HS, Jenkins MC, Allen PC, Harper SB. Characterisation of macrophage migration inhibitory factor from *Eimeria* species infectious to chickens. Mol. Biochem. Parasitol 2007;151:173–183. [PubMed: 17194492]
11. Wu Z, Boonmars T, Nagano I, Nakada T, Takahashi Y. Molecular expression and characterization of a homologue of host cytokine macrophage migration inhibitory factor from *Trichinella* spp. J. Parasitol 2003;89:507–515. [PubMed: 12880250]
12. Cordery DV, Kishore U, Kyes S, Shafi MJ, Watkins KR, Williams TN, Marsh K, Urban BC. Characterization of a *Plasmodium falciparum* macrophage-migration inhibitory factor homologue. J. Infect. Dis 2007;195:905–912. [PubMed: 17299722]
13. Augustijn KD, Kleemann R, Thompson J, Kooistra T, Crawford CE, Reece SE, Pain A, Siebum AHG, Janse CJ, Waters AP. Functional characterization of the *Plasmodium falciparum* and *P. berghei* homologues of macrophage migration inhibitory factor. Infect. Immun 2007;75:1116–1128. [PubMed: 17158894]
14. Starlets D, Gore Y, Binsky I, Haran M, Harpaz N, Shvidel L, Becker-Herman S, Berrebi A, Shachar I. Cell-surface CD74 initiates a signaling cascade leading to cell proliferation and survival. Blood 2006;107:4807–4816. [PubMed: 16484589]
15. Calandra T, Bernhagen J, Mitchell RA, Bucala R. The macrophage is an important and previously unrecognized source of macrophage migration inhibitory factor. J. Exp. Med 1994;179:1895–1902. [PubMed: 8195715]
16. Beverley SM, Ismach RB, Pratt DM. Evolution of the genus *Leishmania* as revealed by comparisons of nuclear-DNA restriction fragment patterns. Proc. Natl. Acad. Sci. USA 1987;84:484–488. [PubMed: 3025876]
17. Saitou N, Nei M. The neighbor-joining method: a new method for reconstructing phylogenetic trees. Mol. Biol. Evol 1987;4:406–425. [PubMed: 3447015]
18. Kumar S, Tamura K, Nei M. MEGA3: integrated software for molecular evolutionary genetics analysis and sequence alignment. Brief Bioinform 2004;5:150–163. [PubMed: 15260895]
19. Poirot O, O'Toole E, Notredame C. Tcoffee@igs: a web server for computing, evaluating, and combining multiple sequence alignments. Nucleic Acids Res 2003;31:3503–3506. [PubMed: 12824354]
20. Leifso K, Cohen-Freue G, Dogra N, Murray A, McMaster WR. Genomic and proteomic expression analysis of *Leishmania* promastigote and amastigote life stages: the *Leishmania* genome is constitutively expressed. Mol. Biochem. Parasitol 2007;152:35–46. [PubMed: 17188763]
21. Ouakad M, Bahi-Jaber N, Chenik M, Dellagi K, Louzir H. Selection of endogenous reference genes for gene expression analysis in *Leishmania major* developmental stages. Parasitol. Res 2007;101:473–477. [PubMed: 17318579]
22. Muller PY, Janovjak H, Miserez AR, Dobbie Z. Processing of gene expression data generated by quantitative real-time RT-PCR. BioTechniques 2002;32:1372–1379. [PubMed: 12074169]
23. Bernhagen J, Mitchell RA, Calandra T, Voelter W, Cerami A, Bucala R. Purification, bioactivity, and secondary structure analysis of mouse and human macrophage migration inhibitory factor (MIF). Biochemistry 1994;33:14144–14155. [PubMed: 7947826]
24. Otwinowski Z, Minor W. Processing of x-ray diffraction data collected in oscillation mode. Macromol. Crystallogr. A 1997;276:307–326.

25. Pape T, Schneider TR. HKL2MAP: a graphical user interface for macromolecular phasing with SHELX programs. J. App. Crystallogr 2004;37:843–844.
26. Sun HW, Bernhagen J, Bucala R, Lolis E. Crystal structure at 2.6-A resolution of human macrophage migration inhibitory factor. Proc. Natl. Acad. Sci. USA 1996;93:5191–5196. [PubMed: 8643551]
27. McRee DE. A visual protein crystallographic software system for X11/XView. J. Mol. Graph 1192;10:44–46.
28. Murshudov GN, Vagin AA, Dodson EJ. Refinement of macromolecular structures by the maximum-likelihood method. Acta Crystallogr. D Biol. Crystallogr 1997;53:240–255. [PubMed: 15299926]
29. Brunger AT, Adams PD, Clore GM, Delano WL, Gros P, Grosse-Kunstleve RW, Jiang JS, Kuszewski J, Nilges M, Pannu NS, et al. Crystallography and NMR system: a new software suite for macromolecular structure determination. Acta Crystallogr. D Biol. Crystallogr 1998;54:905–921. [PubMed: 9757107]
30. Sheldrick GM, Schneider TR. SHELXL: High-resolution refinement. Macromol. Crystallogr. B 1997;277:319–343.
31. Bendrat K, Al-Abed Y, Callaway DJ, Peng T, Calandra T, Metz CN, Bucala R. Biochemical and mutational investigations of the enzymatic activity of macrophage migration inhibitory factor. Biochemistry 1997;36:15356–15362. [PubMed: 9398265]
32. Mason HS. The chemistry of melanin III: mechanism of the oxidation of dihydroxyphenylalanine by tyrosinase. J. Biol. Chem 1948;172:83–99. [PubMed: 18920770]
33. Leng L, Metz C, Fang Y, Xu J, Donnelly S, Baugh J, Delonery T, Chen Y, Mitchell RA, Bucala R. MIF signal transduction initiated by binding to CD74. J. Exp. Med 2003;197:1467–1476. [PubMed: 12782713]
34. Mitchell RA, Liao H, Chesney J, Fingerle-Rowson G, Baugh J, David J, Bucala R. Macrophage migration inhibitory factor (MIF) sustains macrophage proinflammatory function by inhibiting p53: regulatory role in the innate immune response. Proc. Natl. Acad. Sci. USA 2002;99:345–350. [PubMed: 11756671]
35. Mitchell RA, Metz CN, Peng T, Bucala R. Sustained mitogen-activated protein kinase (MAPK) and cytoplasmic phospholipase A_2 activation by macrophage migration inhibitory factor (MIF): regulatory role in cell proliferation and glucocorticoid action. J. Biol. Chem 1999;274:18100–18106. [PubMed: 10364264]
36. Landfear SM, Miller SI, Wirth DF. Transcriptional mapping of *Leishmania enriettii* tubulin messenger-RNAs. Mol. Biochem. Parasitol 1986;21:235–245. [PubMed: 3807944]
38. Nguyen MT, Beck J, Lue HQ, Funfzig H, Kleemann R, Koolwijk P, Kapurniotu A, Bernhagen J. A 16-residue peptide fragment of macrophage migration inhibitory factor, MIF-(50−65), exhibits redox activity and has MIF-like biological functions. J. Biol. Chem 2003;278:33654–33671. [PubMed: 12796500]
38. Swope MD, Lolis E. Macrophage migration inhibitory factor: cytokine, hormone, or enzyme. Rev. Physiol. Biochem. Pharmacol 1999;139:1–32. [PubMed: 10453691]
39. Stamps SL, Fitzgerald MC, Whitman CP. Characterization of the role of the amino-terminal proline in the enzymatic activity catalyzed by macrophage migration inhibitory factor. Biochemistry 1998;37:10195–10202. [PubMed: 9665726]
40. Lubetsky JB, Swope M, Dealwis C, Blake P, Lolis E. Pro-1 of macrophage migration inhibitory factor functions as a catalytic base in the phenylpyruvate tautomerase activity. Biochemistry 1999;38:7346–7354. [PubMed: 10353846]
41. Taylor AB, Johnson WH, Czerwinski RM, Li HS, Hackert ML, Whitman CP. Crystal structure of macrophage migration inhibitory factor complexed with (*E*)-2-fluoro-*p*-hydroxycinnamate at 1.8 A resolution: implications for enzymatic catalysis and inhibition. Biochemistry 1998;38:7444–7454. [PubMed: 10360941]
42. Swope M, Sun HW, Blake PR, Lolis E. Direct link between cytokine activity and a catalytic site for macrophage migration inhibitory factor. EMBO J 1998;17:3534–3541. [PubMed: 9649424]
43. Lubetsky JB, Dios A, Han J, Aljabari B, Ruzsicska B, Mitchell R, Lolis E, Al Abed Y. The tautomerase active site of macrophage migration inhibitory factor is a potential target for discovery of novel anti-inflammatory agents. J. Biol. Chem 2002;277:24976–24982. [PubMed: 11997397]

44. Senter PD, Al-Abed Y, Metz CN, Benigni F, Mitchell RA, Chesney J, Han J, Gartner CG, Nelson SD, Todaro GJ, Bucala R. Inhibition of macrophage migration inhibitory factor (MIF) tautomerase and biological activities by acetaminophen metabolites. Proc. Natl. Acad. Sci. USA 2002;99:144–149. [PubMed: 11773615]
45. David J. Delayed hypersensitivity in vitro: its mediation by cell-free substances formed by lymphoid cell-antigen interaction. Proc. Natl. Acad. Sci. USA 1966;56:72–77. [PubMed: 5229858]
46. Bernhagen J, Krohn R, Lue H, Gregory JL, Zernecke A, Koenen RR, Dewor M, Georgiev I, Schober A, Leng L, et al. MIF is a noncognate ligand of CXC chemokine receptors in inflammatory and atherogenic cell recruitment. Nat. Med 2007;13:587–596. [PubMed: 17435771]
47. Moore KJ, Matlashewski G. Intracellular infection by *Leishmania donovani* inhibits macrophage apoptosis. J. Immunol 1994;152:2930–2937. [PubMed: 8144893]
48. Shi X, Leng L, Wang T, Wang W, Du X, McDonald C, Chen Z, Murphy JW, Lolis E, Noble P, et al. CD44 is the signaling component of the macrophage migration inhibitory factor-CD74 receptor complex. Immunity 2006;25:595–606. [PubMed: 17045821]
49. Poltorak A, Ricciardi-Castagnoli P, Citterio S, Beutler B. Physical contact between lipopolysaccharide and Toll-like receptor 4 revealed by genetic complementation. Proc. Natl. Acad. Sci. USA 2000;97:2163–2167. [PubMed: 10681462]
50. Mitchell RA, Liao H, Chesney J, Fingerle-Rowson G, Baugh J, David J, Bucala R. Macrophage migration inhibitory factor (MIF) sustains macrophage proinflammatory function by inhibiting p53: regulatory role in the innate immune response. Proc. Natl. Acad. Sci. USA 2002;99:345–350. [PubMed: 11756671]
51. Suzuki M, Sugimoto H, Nakagawa A, Tenaka I, Nishihira J, Sakai M. Crystal structure of the macrophage migration inhibitory factor from rat liver. Nat. Struct. Biol 1996;3:259–266. [PubMed: 8605628]
52. Bucala R, Lolis E. MIF: a critical component of autoimmune inflammatory diseases. Drug News Perspect 2005;18:417–426. [PubMed: 16362080]
53. Flieger O, Engling A, Bucala R, Lue HQ, Nickel W, Bernhagen J. Regulated secretion of macrophage migration inhibitory factor is mediated by a non-classical pathway involving an ABC transporter. FEBS Lett 2003;551:78–86. [PubMed: 12965208]
54. Kleemann R, Hausser A, Geiger G, Mischke R, Burger-Kentischer A, Flieger O, Johannes FJ, Roger T, Calandra T, Kapurniotu A, et al. Intracellular action of the cytokine MIF to modulate AP-1 activity and the cell cycle through Jab1. Nature 2000;408:211–216. [PubMed: 11089976]
55. Juttner S, Bernhagen J, Metz CN, Rollinghoff M, Bucala R, Gessner A. Migration inhibitory factor induces killing of *Leishmania major* by macrophages: dependence on reactive nitrogen intermediates and endogenous TNF-α. J. Immunol 1998;161:2383–2390. [PubMed: 9725234]
56. Marson AL, Tarr DE, Scott AL. Macrophage migration inhibitory factor (mif) transcription is significantly elevated in *Caenorhabditis elegans* dauer larvae. Gene 2001;278:53–62. [PubMed: 11707322]
57. Notredame C, Higgins DG, Heringa J. T-Coffee: a novel method for fast and accurate multiple sequence alignment. J. Mol. Biol 2000;302:205–217. [PubMed: 10964570]
58. Kraulis PJ. Molscript: a program to produce both detailed and schematic plots of protein structures. J. Appl. Crystallogr 1991;24:946–950.
59. Delano, W. The PyMOL Molecular Graphics System. DeLano Scientific; San Carlos, CA: 2002.
60. Christopher, JA. SPOCK: the Structural Properties Observation and Calculation Kit Program Manual. Center for Macromolecular Design. Texas A&M University; College Station, TX: 1998. 1998.

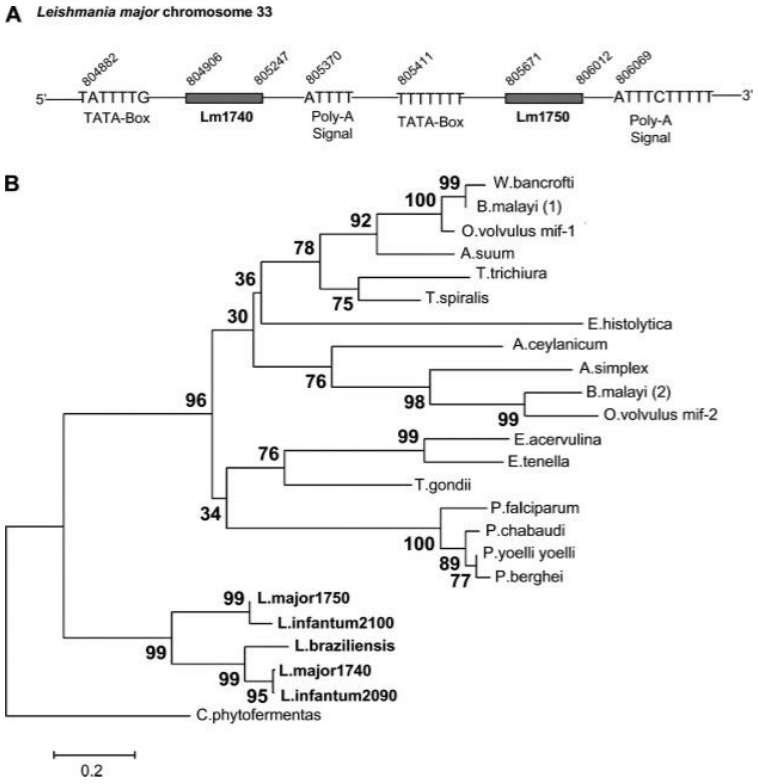

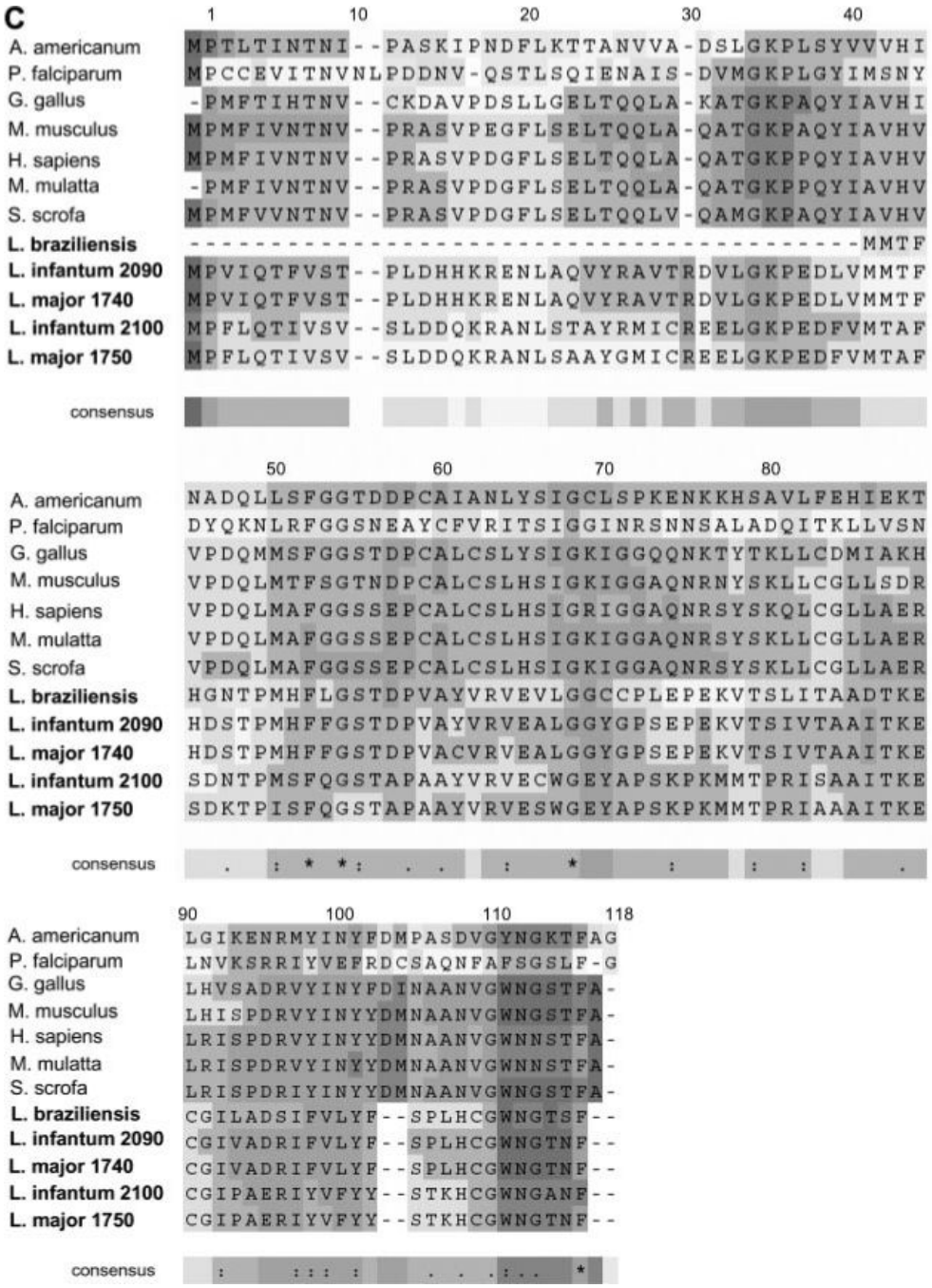

FIGURE 1.

MIF-like sequences in *Leishmania*. *A*, Physical map of the *L. major* chromosome 33 region encompassing nucleotides 804882−806078. The two *mif*-related genes, Lm1740 (accession number Q4Q413) and Lm1750 (accession number Q4Q413) are shown together with consensus TATA-boxes and poly-adenylation signal sequences. *B*, Phylogram of parasitic MIF protein sequences including five *mif*-related proteins identified in the *Leishmania* species *L. major*, *L. infantum*, and *L. braziliensi*s. The sequence of *C. phytofermentas* was used to resolve relationships among MIF-expressing parasites. The percentage of replicate trees in which the associated taxa clustered together in the bootstrap test (5000 replicates) are shown next to the branches. The evolutionary distances were computed using the Poisson correction method and

are in the units of the number of amino acid substitutions per site. The gene accession numbers are: *L. infantum,* 2100 XM_001468253; *L. infantum,* 2090 XM_001468252; *L. braziliensis,* CAM40731; *L. major1740,* Q4Q413; *L. major1750,* Q4Q412′ *Toxoplasma gondii,* DQ344450; *Eimeria acervulina,* DQ323516; *Eimeria tenella,* DQ323515; *Ancyloxypha simplex,* EF165010; *Wichereria bancrofti,* AF040629; *Plasmodium yoelli yoelli,* DQ494171; *Plasmodium falciparum,* AY561832; *Plasmodium chabaudi,* CAH75532; *Plasmodium berghei,* CAH99597; *Trichuris trichiura,* AJ237770; *Trichinella spiralis,* AY050661; *Ascaris suum,* AB158366; *Entamoeba histolytica,* XM_650516; *A. ceylanicum,* EF410151; *B. malayi (1),* AF002699; B. malayi (2), AY004865; Onchocerca volvulus mif-1. AF384027; O. volvulus mif-2, *AF384028. C,* Amino acid sequence alignment of selected MIF molecules constructed with the program T-Coffee (19). The consensus line indicates for each residue: *, complete conservation; :, conservation of residue size and hydropathy; ., conservation of size or hydropathy. The color code evaluates the consistency between a multiple alignment and every pair of aligned residues (59). Medium gray box, inconsistent bits, unlikely to be correctly aligned; light gray, medium gray, and dark gray boxes, bits correspond to the residues more likely to be correctly aligned (with dark gray the highest reliable portion). The consensus indicates the average reliability value for every residue column. The additional gene accession numbers are: *A. americanum,* Q9GUA9; *Gallus gallus,* Q02960; *Mus musculus,* P34884; *Homo sapiens,* Q6FHV0; *Macaca mulatto,* Q6DN04; *Sus scrofa,* Q069I4.

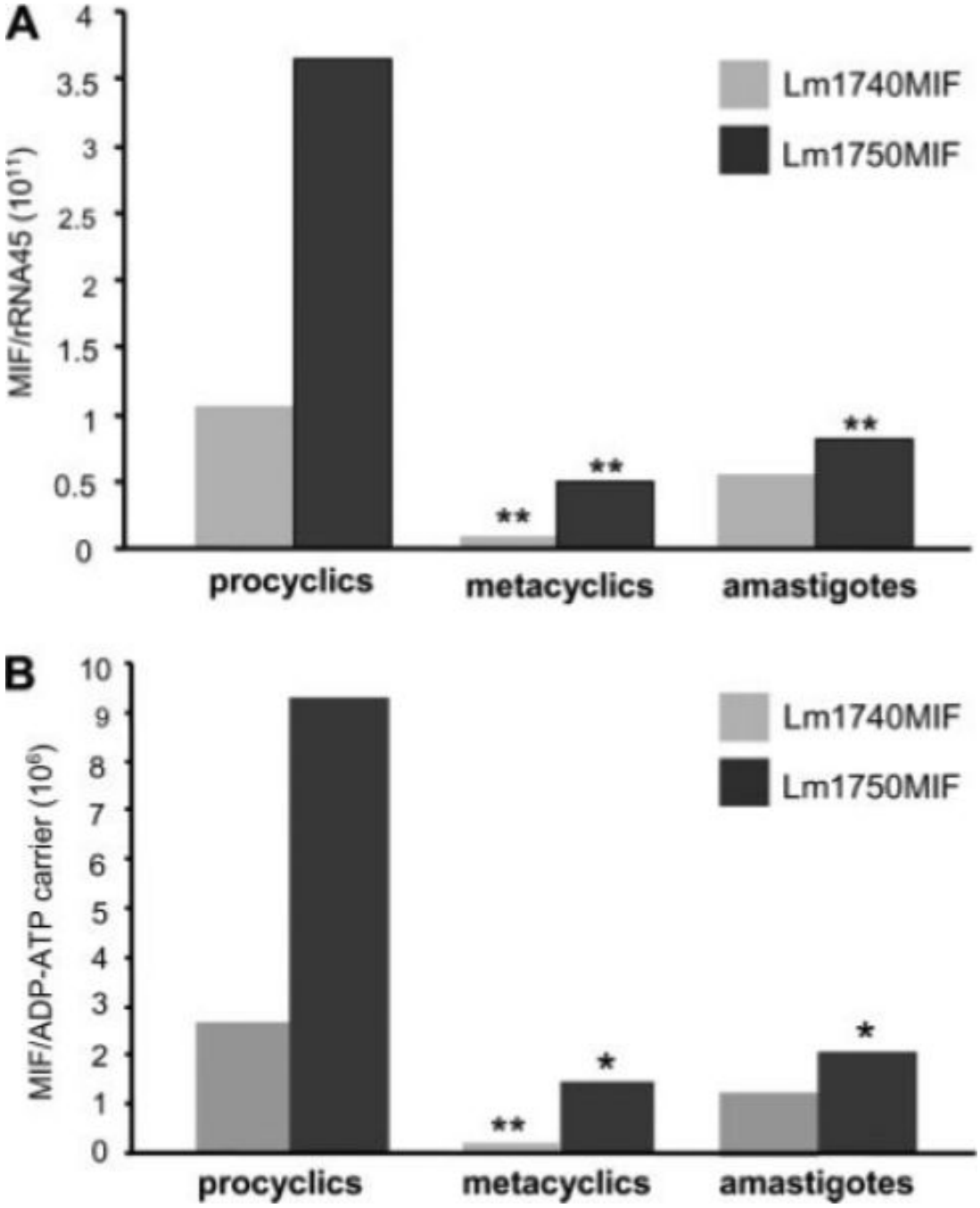

FIGURE 2.

Lm1740MIF and Lm1750MIF mRNA are expressed by *L. major*. Real-time qPCR analysis of total RNA from *L. major* procyclic and metacyclic forms cultured in vitro, and from amastigotes present within the infected lymph nodes of mice. Experiments were conducted for Lm1740MIF and Lm1750MIF transcripts relative to the internal control mRNAs, rRNA45 (*A*) and ADP/ATP carrier (*B*). All samples were run in triplicates. The *p* values were calculated by Student's *t* test **, $p < 0.01$ for procyclics vs metacyclics or amastigotes; *, $p < 0.05$ for procyclics vs metacyclics or amastigotes.

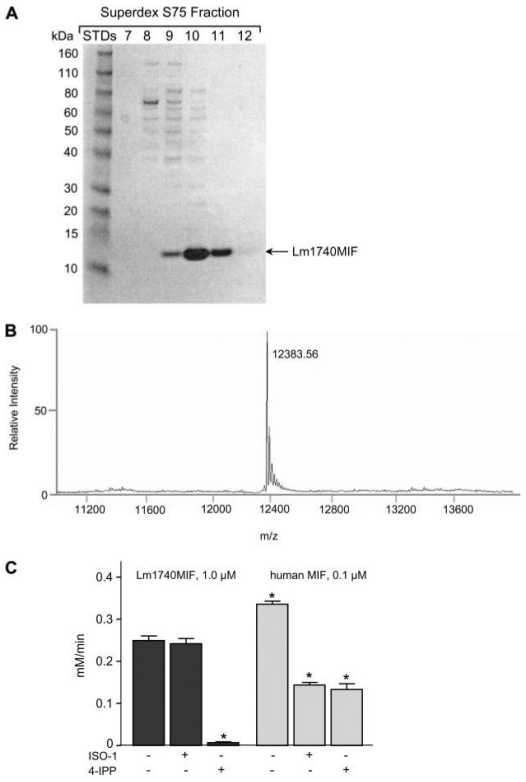

FIGURE 3.

Biochemical characterization of the Lm1740MIF protein. *A*, SDS/PAGE and Coomassie staining analysis of recombinant Lm1740MIF protein fractions eluted from size exclusion chromatography on a Superdex 75 10/300 GL column. STDs, protein molecular mass standards. *B*, Electrospray ionization mass spectrometry of Lm1740MIF showing a molecular mass (*m/z*) that lies within 0.02% accuracy of the predicted *m/z* (12381.22 Da). *C*, Tautomerization activity of Lm1740MIF and human MIF measured with the substrate, D-dopachrome methyl ester. A representative reaction is shown for Lm1740MIF at 1 μM and for human MIF at 0.1 μM. The small-molecule inhibitors ISO-1 or 4-IPP were preincubated with MIF at 1000- or 1-fold molar excess, respectively. The lower tautomerase activity of Lm1740MIF made it necessary to use a higher concentration of this protein for the inhibition studies. Data are means ± SD of triplicate measurements. The *p* values were calculated by Student's *t* test. *, $p < 0.001$ for human MIF vs Lm1740MIF, for 4-IPP-treated Lm1740MIF vs untreated Lm1740MIF, for ISO-1- or 4-IPP-treated human MIF vs untreated human MIF, and for 4-IPP-treated Lm1740MIF vs 4-IPP-treated human MIF.

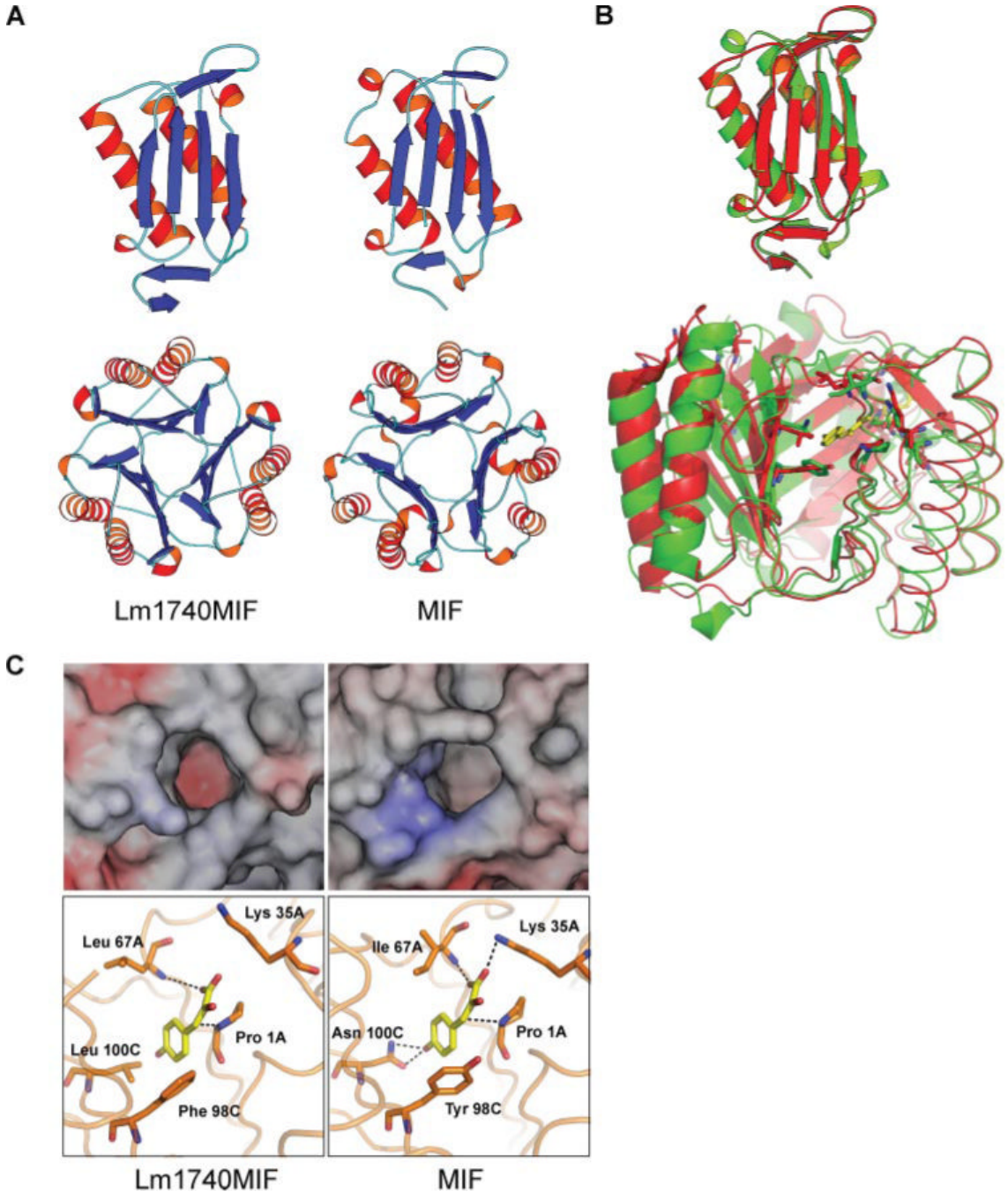

FIGURE 4.

Conserved structure between Lm1740MIF and MIF. *A*, Schematic representation of the Lm1740MIF and human MIF protomers (*top*) and trimers (*bottom*) with secondary structure elements shown in blue (β sheet), red (α helix) and cyan (random coil). *B*, Superim-position of the backbone ribbon diagrams of monomeric and trimeric Lm1740MIF (red) and human MIF (green). In the trimeric representation, one of the protomers is displayed as backbone trace. Also shown in the trimer representation are the side chain residues implicated in substrate recognition. The substrate *p*-hydroxyphenylpyruvate is displayed in yellow. *C*, Electrostatic surface potential of the tautomerase site of Lm1740MIF and human MIF (*top*). The negatively charged surface potential is displayed in red and the positive potential in blue. Molecular model

of active site residues implicated in substrate contact for Lm1740MIF based on a crystal structure of MIF complexed with *p*-hydoxyphenylpyruvate (*bottom*; Ref. 40). Residue numbering refers to sequence alignment of Fig. 1*C*. The program Molscript (58) was used to prepare *A*, PyMOL (59) was used to prepare *B* and *C* (*lower panels*), and SPOCK (60) was used to generate *C* (*upper panels*).

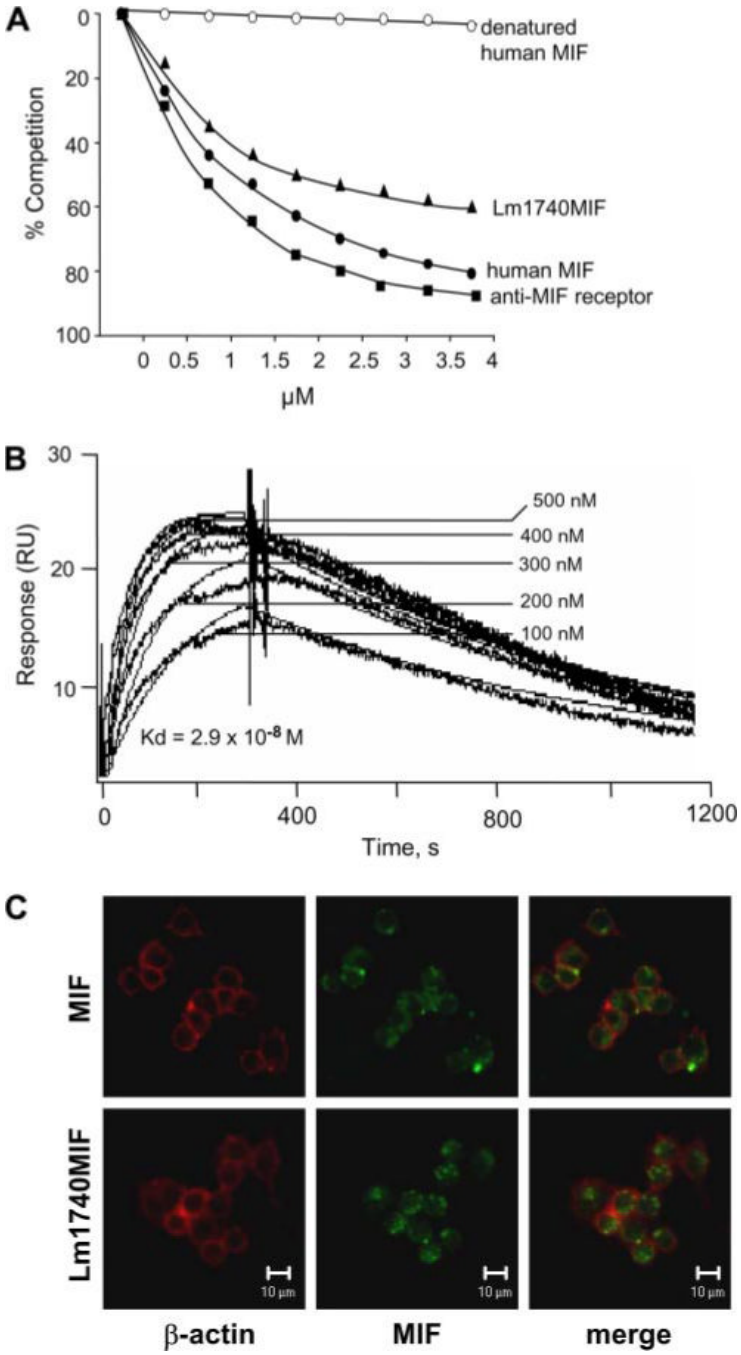

FIGURE 5.

Lm1740MIF binds to the MIF receptor, CD74, and is internalized by macrophages. *A*, Concentration-dependent binding of Lm1740MIF and human MIF to the immobilized, human MIF receptor ectodomain (sCD74) using biotinylated human MIF as a competitor. A neutralizing anti-MIF receptor mAb (LN2) and heat-denatured, recombinant human MIF served as positive and negative controls for this assay. Values are the means of quadruplicate measurements. *B*, Real-time surface plasmon resonance analysis (BIAcore) of the interaction between recombinant Lm1740MIF and sCD74. *C*, Exogenously added Lm1740MIF is internalized by RAW 264.7 macrophages. Fluorescein-labeled Lm1740MIF or human MIF

(green) was added to the cells at 1.5 μM, and staining for β-actin (red) was performed 30 min later as described in *Materials and Methods*.

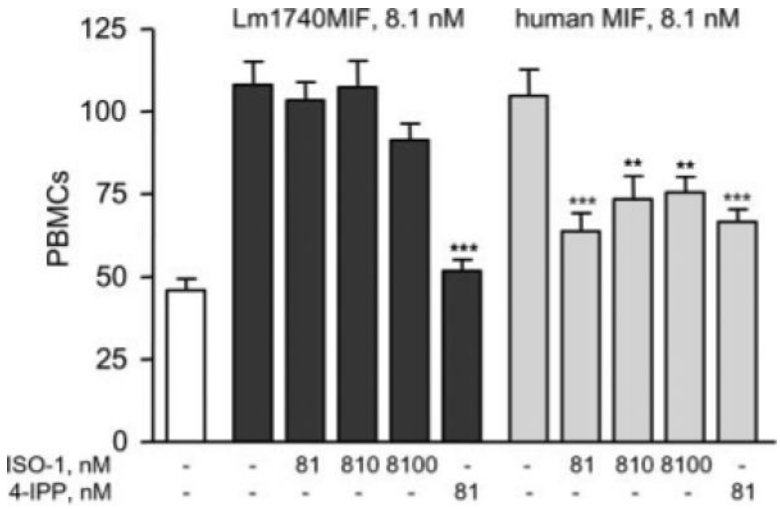

FIGURE 6.

Lm1740MIF induces mononuclear cell migration. Human PBMCs were subjected to migration analysis with or without 8.1 nM (100 ng/ml) recombinant Lm1740MIF in the lower chamber. Human MIF served as positive control. The MIF inhibitor ISO-1 was added in 10-, 100-, and 1000-fold molar excess to the recombinant protein, and the inhibitor 4-IPP was added in 10-fold molar excess. Results are representative of 2 independent experiments and are expressed as the mean number of 12 counted fields ± SE. The *p* values were calculated by Student's *t* test. **, $p < 0.01$, ***, $p < 0.001$. for Lm1740 or human MIF vs protein with inhibitors.

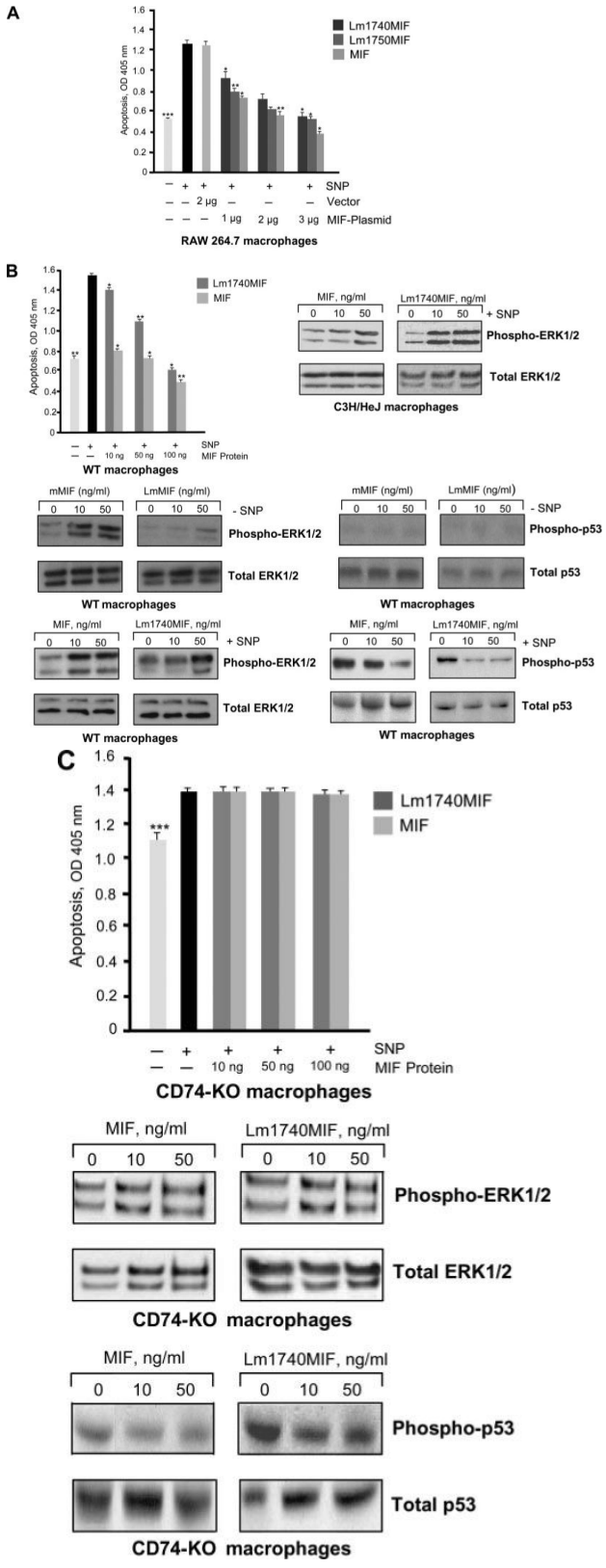

FIGURE 7.

LmMIF protects macrophages from apoptosis and activates signal transduction in a MIF receptor-dependent manner. *A*, Murine RAW264.7 monocytes were transfected with plasmids encoding Lm1740MIF, Lm1750MIF, murine MIF (MIF), or a control vector. The NO donor, SNP, was added 20 h later, and DNA fragmentation was assessed by ELISA. Data are the means ± SD of five experiments. The *p* values were calculated by Student's *t* test. **, $p < 0.01$, *, $p < 0.05$ for MIF vs vector control. **, $p < 0.01$, *, $p < 0.05$ for Lm1740MIF vs MIF and for Lm1750MIF vs MIF. ***, $p < 0.001$ for RAW264.7 vs vector control treated with SNP. The values for $p > 0.05$ are not displayed. *B*, Wild-type (WT) BMMs were treated with Lm1740MIF or murine MIF at the concentrations shown before the addition of the apoptosis inducer, SNP. DNA fragmentation was assessed by ELISA 36 h later. The *p* values were calculated by Student's *t* test. **, $p < 0.01$, *, $p < 0.05$ for MIF vs SNP control. **, $p < 0.01$, **, $p < 0.05$ for Lm1740MIF vs MIF. **, $p < 0.01$ for control vs SNP addition. The values for $p > 0.05$ are not displayed. The phosphorylation of ERK1/2 and p53 was assessed by Western blotting using specific phospho-ERK1/2, total ERK1/2, phospho-p53, and total p53 Abs. BMMs were treated with the NO donor SNP, as indicated. Western blotting for phosphorylation of ERK1/2 of C3H/HeJ bone marrow macrophages served as a control against LPS contamination. *C*, BMMs from MIF receptor-deficient (CD74-KO) mice were prepared and studied for protection from apoptosis, ERK1/2 phosphorylation, and phospho-p53 content as in *B*. The *p* values were calculated by Student's *t* test. ***, $p < 0.001$ for control vs SNP addition. The *p* values for comparisons with $p > 0.05$ are not displayed. Both the apoptosis studies and the Western blots are representative of at least four independently performed experiments.

Table I

Data collection and refinement statistics

	Native	Selenomethionylated Crystal		
Data collection				
Space group	R3	R3		
Cell dimensions				
a, *b*, *c* (Å)	52.32, 52.32, 96.82	52.11, 52.11, 96.83		
α, *β*, *γ* (degrees)	90, 90, 120	90, 90, 120		
		Peak	*Inflection*	*Remote*
Wavelength (Å)	0.95	0.97912	0.97928	0.96389
Resolution (Å)	50−1.03 (1.07−1.03)[a]	1.6	1.6	1.6
R_{sym} or R_{merge}	0.051 (0.228)	0.066	0.051	0.052
$I/\sigma I$	22 (6.8)	6.4	6.8	6.6
Completeness (%)	95.5 (71.6)	99.7	99.6	99.7
Redundancy	5.2 (3.4)	7.2	7.2	7.3
Refinement				
Resolution (Å)	10−1.03			
No. of reflections	44,388			
R_{work}/R_{free}	0.139/0.157			
N. of atoms	1,004			
Protein	880			
Ligand/ion	4			
Water	120			
B factors				
Protein	14.2			
Ligand/ion	40			
Water	28.7			
Root mean square deviations				
Bond lengths (Å)	0.016			
Bond angles (degrees)	2.1			
Ramachandran plot (%)[b]				
Most favored	94.7			
Allowed	5.4			

[a] Numbers in parentheses, highest resolution shell.

[b] As defined in PROCHECK.